3BTRON: A Blood-Brain Barrier Recognition Network

Nan Fletcher-Lloyd[1, 2, †], Isabel Bravo-Ferrer[4, 5, •], Katrine Gaasdal-Bech[4, 5, 6], Blanca Díaz Castro[4, 5, 6], and Payam Barnaghi[1, 2, 3, 7]

[†] *Corresponding author*
[1] *Imperial College London*
[2] *UK Dementia Research Institute, Care Research and Technology Centre*
[3] *University College London*
[4] *Centre for Discovery Brain Sciences, The University of Edinburgh*
[5] *UK Dementia Research Institute, The University of Edinburgh*
[•] *Current affiliation is University College London*
[6] *British Heart Foundation and UK Dementia Research Institute Centre for Vascular Dementia Research*
[7] *Great Ormond Street Hospital NHS Foundation Trust*

Abstract

The blood-brain barrier (BBB) plays a crucial role in maintaining brain homeostasis. During ageing, the BBB undergoes structural alterations. Electron microscopy (EM) is the gold standard for studying the structural alterations of the brain vasculature. However, analysis of EM images is time-intensive and can be prone to selection bias, limiting our understanding of the structural effect of ageing on the BBB. Here, we introduce 3BTRON, a deep learning framework for the automated analysis of the BBB architecture (the morphology, structure, and texture of its various components) in EM images. Using age as a readout, we trained and validated our model on a unique dataset (n = 359). We show that the proposed model could confidently identify the BBB architecture of aged mouse brains from young mouse brains across three different brain regions, achieving a sensitivity of 77.8% and specificity of 80.0% post-stratification when predicting on unseen data. Additionally, feature importance methods revealed the spatial features of each image that contributed most to the predictions. These findings demonstrate a new data-driven approach to analysing age-related changes in the architecture of the BBB.

Main

The blood vessels of the brain, unlike the vasculature in other organs, form a unique structure that tightly controls the exchange of substances between the blood and the brain parenchyma,

thereby maintaining brain homeostasis. This structure is known as the blood-brain barrier (BBB). The BBB is comprised of the brain endothelial cells, which form the blood vessel wall and are tightly sealed by highly specialised intercellular junctions (tight junctions), supported by mural cells (smooth muscle cells and pericytes), astrocyte processes (endfeet), and the extracellular matrix (basement membrane) that surrounds them.[1] Ageing is accompanied by changes in the structure and function of the BBB.[2,3] Among these age-related changes are an increased BBB permeability to exogenous dyes[4,5] and increased transcytosis and molecular remodelling.[6] At the subcelluar (ultrastructural) level, several studies have revealed changes in specific parameters such as tight junction tortuosity or basement membrane thickness.[7,8] However, the labour-intensive nature of analysing BBB ultrastructure images has limited a detailed understanding of the structural effect of ageing on the BBB and how this may contribute to BBB dysfunction. As ageing is considered a major risk factor for most neurodegenerative diseases,[9] and vascular dysfunction is an early hallmark of diseases that lead to dementia,[10,11] there is an unmet need for tools that allow for rapid, large-scale analysis to gain deeper insights into the impact of ageing on this crucial functional barrier.

While magnetic resolution imaging (MRI) studies have been able to uncover larger-scale changes in brain vasculature due to age,[12-14] the spatial resolution of MRI, in the order of millimetres, makes the technique unsuitable to capture changes occurring at the cellular and sub-cellular level. Similarly, light microscopy studies, with a spatial resolution of around 250 nm, have demonstrated how ageing affects overall brain vascular structure.[5,15] However, the BBB is composed of many components that are below 250 nm in size, e.g. tight junctions, basement membrane, or astrocyte endfeet. Thus, higher resolution microscopy is needed to quantify changes in these components. By contrast, electron microscopy (EM) can achieve sub-nanometre resolution, making it the preferred method by which to study the impact of age, injury and disease at the BBB ultrastructural level. Indeed, EM analyses have revealed several such changes in the vasculature of the ageing and diseased brains of both rodents and humans.[8,14,16-18] The downside of using EM is that analysis requires significant manual work which is highly time-consuming, leading to the unavoidable selection of very specific measurements to quantify, limiting the scope of the studies to a reduced number of structures, biological replicates, or brain areas. Furthermore, this type of analysis is susceptible to personal bias, as interpretation may be influenced by pre-existing hypotheses held by the researcher, leading to the skewed selection of evidence. As such, there is a need for an efficient method that can minimise subjectivity and provide a more rigorous and unbiased analysis.

The advent of deep learning techniques, particularly Deep Convolution Neural Networks (DCNNs), in the field of machine learning has revolutionised the automation of cell image analysis. Unlike traditional machine learning, these models use multi-layer hierarchical feature extraction, making them more suitable for processing complex morphology for classification, detection, and segmentation.[19] In the last few years, several studies have leveraged deep learning techniques to study brain cells. Suleymanova *et al.* applied a DCNN-based method to count the number of astrocytes in different brain regions of rats in immunohistological images. Kayasandik *et al.* took this work one step further, using multiscale directional

filters for improved astrocyte detection in fluorescent microscopy images of mouse brains. Most recently, Heckenbach *et al.* presented deep learning models that could predict cellular senescence based on nuclear morphology. Nuclei were detected using the image segmentation network U-Net, before a predictor was used to generate senescence scores in human fibroblasts.[20] They also showed that their model could identify senescence in murine astrocytes among other cell types. Deep learning has also been used to study BBB function, primarily focusing on improving the predictability of its permeability to support the discovery of drug compounds able to cross the BBB.[21–26] Importantly, however, no studies have yet applied deep learning techniques to study the BBB at a structural level. Inspired by these works, our goal was to develop a deep learning model that could classify BBB electron microscopy images from aged mouse brains based on the BBB architecture, which we define as the morphology, structure and texture of its various components.

This study presents 3BTRON: A Blood-Brain Barrier Recognition Network for analysing BBB architecture in electron microscopy images. As a proof-of-concept, we demonstrate the utility of 3BTRON applied to the identification of the BBB architecture of the brains of aged mice, establishing its potential as an investigative tool. Through optimisation, we establish stratification thresholds for age likelihood to enhance the network's flexibility for contextual translation, before using feature importance to reveal the parts of each image that contribute most towards the age likelihood score predicted for that image. The proposed approach has been evaluated on a dataset of 359 images taken from 23 mice (Figure 1 presents an overview).

Our work offers an automated framework for analysing BBB architecture in different brain regions. The use of high-resolution image data combined with deep transfer learning results in a high-throughput pipeline that can be used to support research into the BBB with increased efficiency. By providing a standardised, data-driven assessment of the BBB architecture, this framework ensures greater reliability and generalisability of findings. In the context of ageing, our model can be used as a tool to investigate researcher hypotheses, for example, by guiding the discovery of age-related changes to the BBB architecture that may lead to the brain's regional vulnerability to neurodegenerative diseases, or to efficiently assess the effectivity of treatments targeting vascular ageing at the BBB structural level.

Results

Model performance

We evaluated and compared the effectiveness of our model using four different architectures to extract image features: Resnet50, MobileNetv2, VGG16, and VGG19. We found the best-performing classification model was ResNet50 with L2 regularisation. Table 1 presents this model performance on both the validation and test data (definitions of evaluation metrics can be found in Supplementary Information Section 3). Results from the other models are included in Supplementary Information Table 1 in Supplementary Information Section 6. We also report the difference in mean predicted probabilities between images that the model

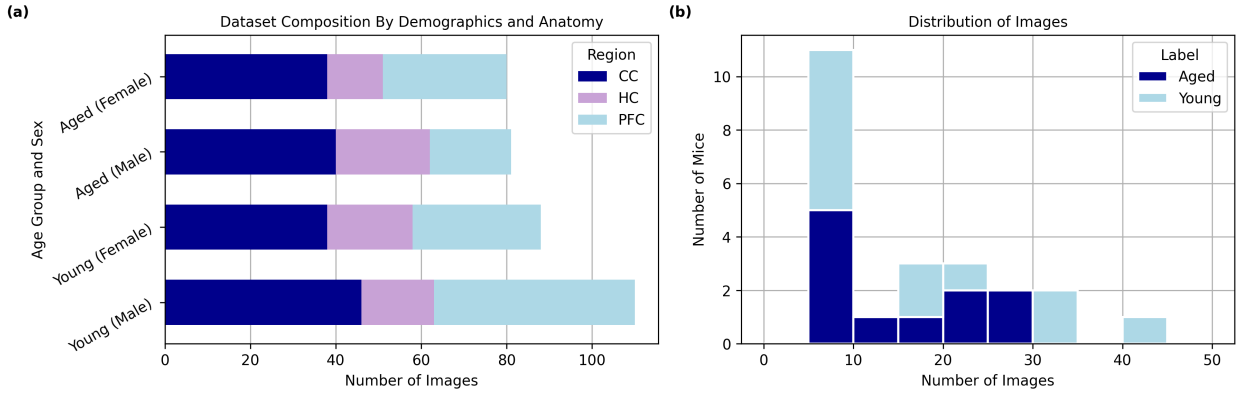

Figure 1: The dataset. a) The number of images collected per brain region (corpus callosum – CC, hippocampus – HC, or prefrontal cortex – PFC) for each age group and sex. b) The distribution of image data by mouse. We see that the vast majority of images have been collected from different mice, which will reduce bias from overfitting in the model.

has classified as young and aged (after stratification) for each sex and brain region (see Tables 2 and 3). Analysis of model reliability and calibration can be seen in Supplementary Information Figure 3 in Supplementary Information Section 7.

Table 1: Mean (95% CI) % of sensitivity, specificity, and area under the precision-recall curve of the prediction model on the different data splits. These results are reported before and after stratification is performed.

Before Stratification

	Sensitivity	**Specificity**	**AUC Precision-Recall**
Validation	67.6 (65.2 - 69.9)	72.6 (69.4 - 75.8)	76.7 (73.8 - 79.7)
Test	68.8	52.6	63.9

After Stratification

	Sensitivity	**Specificity**	**Precision**
Validation	79.0 (75.5 - 82.5)	79.5 (75.3 - 83.6)	76.7 (72.2 - 81.2)
Test	77.8	80.0	77.8

Stratification of age likelihood

We calculated stratified age likelihood scores as discussed in Section: Stratification of Age Scores for Reporting Model Uncertainty. By varying the stratification thresholds, we were able to balance the sensitivity and specificity for the 'Green' (young) and 'Red' (aged)

groups, while limiting the number of samples about which the model could not confidently predict. Here, we select thresholds [0%, 25%], [25%, 75%], and [75%, 100%] (following interval notation) for the 'Green', 'Amber', and 'Red' groups, respectively. Table 1 shows the model performance after stratification when grouping the predictions on the 'Green' and 'Red' groups. Figure 2 reports the distribution of the model's predictions by group (including the 'Amber' group) on the test set. Additionally, in Supplementary Information Section 9, we compare model performance across tissues from different brain regions and male and female mice (see Supplementary Information Tables 2 and 3).

Table 2: Difference in mean predicted probability for images classified as young and aged by the model for each sex after stratification.

Sex	Aged	Young	Difference
Female	88.5	17.3	71.3
Male	90.1	15.6	74.5

Table 3: Difference in mean predicted probability for images classified as young and aged by the model for each brain region (corpus callosum – CC, hippocampus – HC, or prefrontal cortex – PFC) after stratification.

Brain Region	Aged	Young	Difference
CC	92.6	22.7	69.9
HC	83.4	16.7	66.6
PFC	87.4	12.5	74.9

Feature importance

The most important regions influencing predictions according to the convolutional layers were identified using Gradient-weighted Class Activation Mapping (Grad-CAM), a technique used in deep learning for producing explainable predictions and calculating contributions from the spatial features of images.[27] Here, we show Grad-CAM visualisations generated from two different layers of the neural network, one representing low-level features (e.g. edges, textures and shapes) captured in the early layers of the model, and one representing high-level semantic features (e.g. objects or parts of objects) captured in the deeper layers of the model, with warm colours (red or yellow) showing regions of the image to which the model has paid the most attention and cool colours (blue or green) indicating areas that were less important to the final decision. This approach allowed us to breakdown the prediction made for each image and to better understand the contributions to the age likelihood score. Figure 3 shows this breakdown on three images from the test set: a correctly predicted

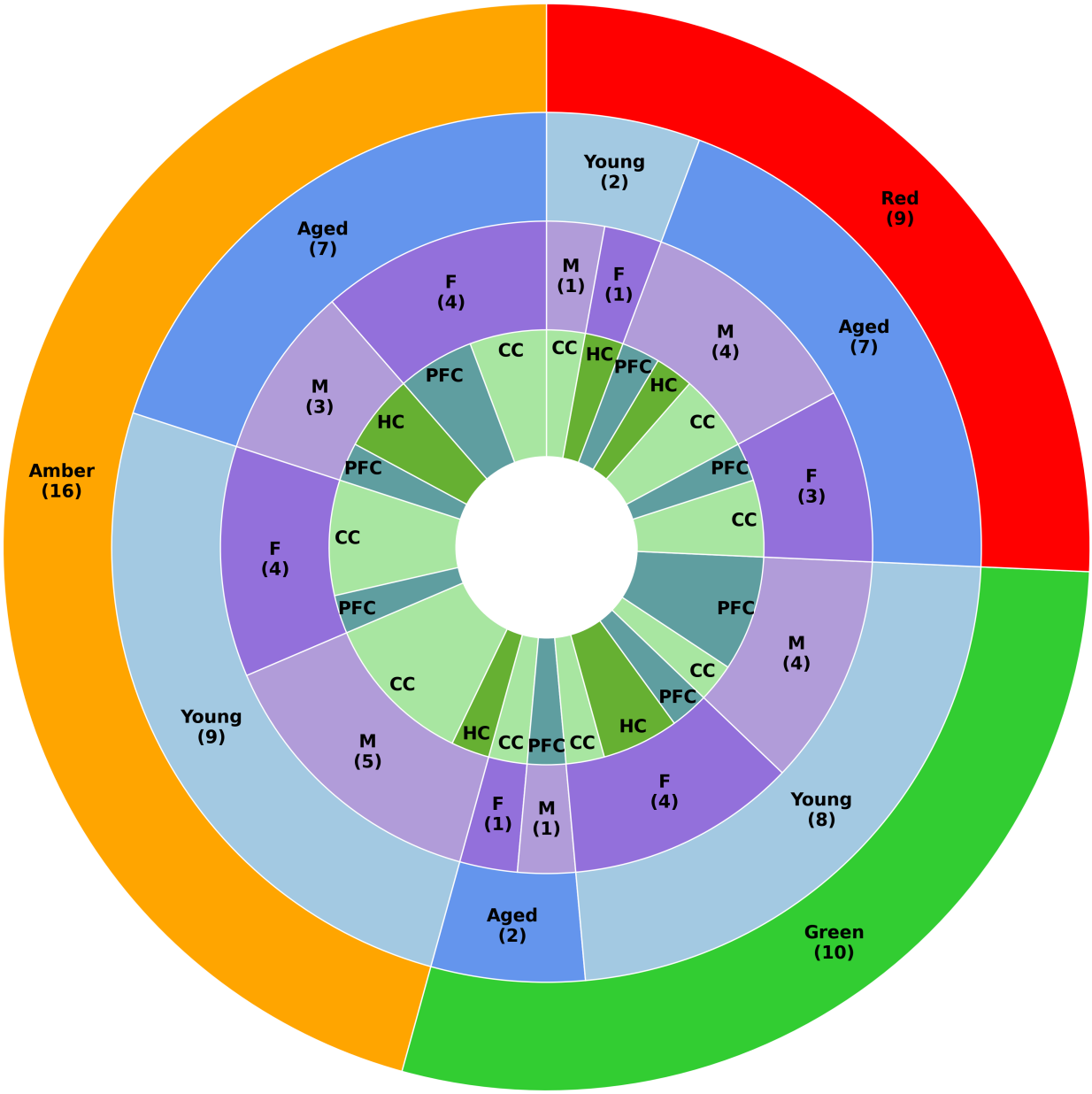

Figure 2: Final Model Stratification Breakdown. Analysis of stratified groupings produced by evaluating the final model on the held-out test set using optimised thresholds. 'Green' represents the samples that the model confidently predicts are from a young mouse, 'Amber' the samples that the model is not confidently predicting, and 'Red' the samples that the model confidently predicts are from an aged mouse. Each group is further broken down by the true age of the samples, then by the sex of the mouse (female – F/male – M), and finally by brain region (corpus callosum – CC, hippocampus – HC, or prefrontal cortex – PFC).

certain positive (aged) example, a correctly predicted certain negative (young) example, and an example that the model could not confidently predict.

The middle-age brain

We also applied the final trained model to an unlabelled dataset of 52 images from the brains of 3 middle-age (366 days) female mice taken from the corpus callosum and prefrontal cortex. In table 4 , we report the percentage of images predicted as young and aged for each brain region, as well as the percentage of images about which the model was uncertain. Figure 4 shows the breakdown of the model's predictions on three images using Grad-CAM heatmaps: an image predicted positive (aged), an image predicted negative (young), and an image that the model could not confidently predict.

Table 4: Percentage of images predicted young and aged for each brain region (corpus callosum - CC and prefrontal cortex - PFC), as well as the percentage of images about which the model was uncertain.

Brain Region	**Total Images**	**Aged**	**Young**	**Uncertain**
CC	29	55.2	13.8	31.0
PFC	23	26.1	8.7	65.2

Discussion

The BBB plays a crucial role in maintaining brain health and function. Indeed, the breakdown of the BBB has been recognised as an early biomarker for human cognitive dysfunction.[28] Therefore, to better understand how the ageing process increases vulnerability to disease, it is essential to unveil the impact of ageing on the architecture of the BBB. Moreover, given the different susceptibilities of brain regions to various types of pathology, it is important to explore regional differences during ageing. By developing an explainable automated approach to analysing the BBB architecture in different brain regions of aged mice, we contribute a framework to directly address this priority.

We present a deep transfer learning pipeline for estimating age likelihood using electron microscopy image data, combined with demographic and anatomical data. We considered several deep learning models for image feature extraction and found that ResNet50 attained the top performance (sensitivity of 68.8% and specificity of 52.6%). The ratios of positives (images from aged mice) to negatives (images from young mice) in the test set is $1 : 1.25$. Through stratification, age likelihood scores were transformed into three tuneable groups allowing us flexibility in the management of model accuracy and fairness. Following this, the performance on the 'Green' and 'Red' groups was significantly improved, achieving a sensitivity of 77.8%, and a specificity of 80.0% (see Supplementary Information Section 3

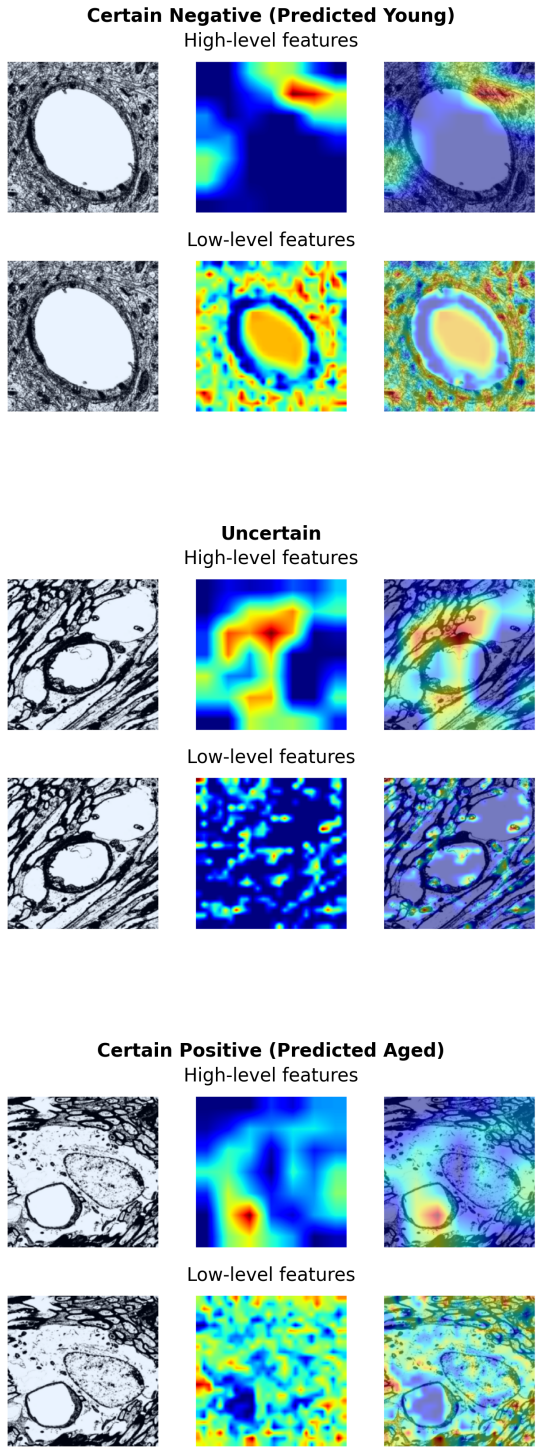

Figure 3: Visualisations of contributing spatial features for early-stage and final classification of images from young and aged mice. Overlaid Gradient-weighted Class Activation Mapping heatmaps show how strongly different regions of each input image contribute to the specific class prediction given to that image by the final model. Warm colours (red or yellow) show regions to which the model has paid the most attention and cool colours (blue or green) indicate areas that were less important to the final decision.

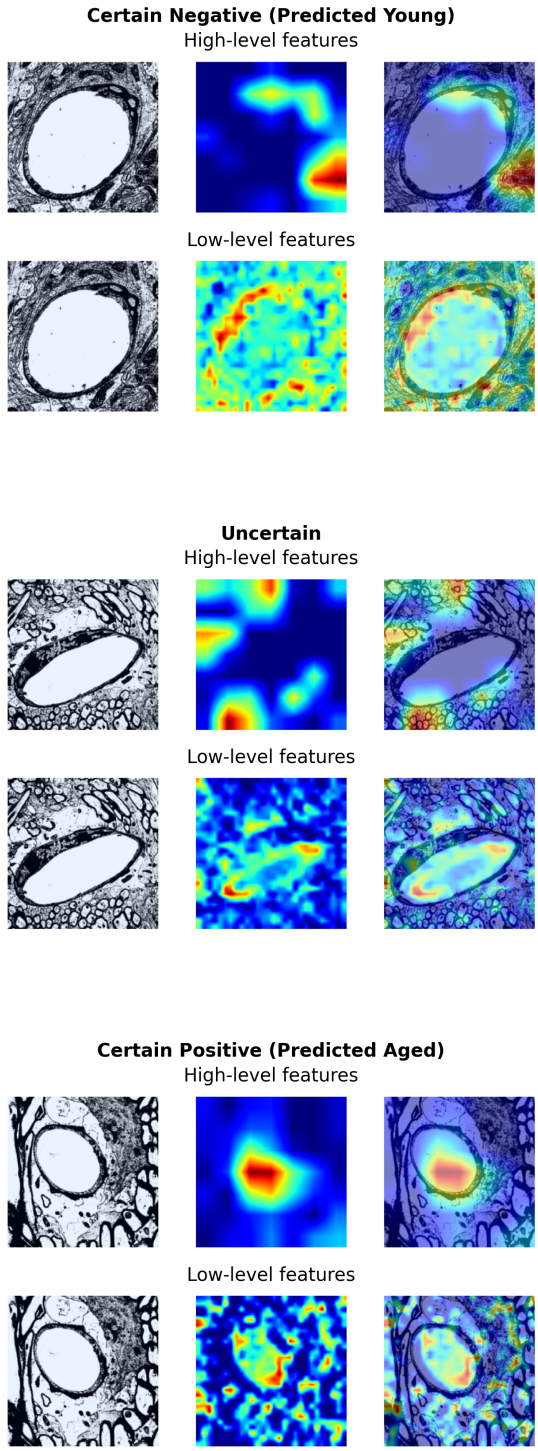

Figure 4: Visualisations of contributing spatial features for early-stage and final classification of images from middle-age mice. Overlaid Gradient-weighted Class Activation Mapping heatmaps show how strongly different regions of each input image contribute to the specific class prediction given to that image by the final model. Warm colours (red or yellow) show regions to which the model has paid the most attention and cool colours (blue or green) areas that were less important to the final decision.

for definitions of evaluation metrics). A breakdown of these predictions as seen in Figure 2 and Tables 2 and 3 in Supplementary Information Section 9 showed that re-grouping the model's predictions based on the age likelihood score ensured similar levels of accuracy were achieved in each sex and across all three brain regions. While these thresholds increased model uncertainty, we chose to prioritise correct certain predictions for the purposes of this research scenario. When we applied our model to a dataset taken from middle-age female mice, very few images were classified as young, while the model was uncertain or classified images as aged at relatively equal rates across the whole dataset. Considering brain region, we see that just over half of the images from the corpus callosum were classified as aged, while the model was uncertain about the majority of the images from the prefrontal cortex (see Table 4). The application of our framework to middle-age mouse brains emphasises its potential to help reveal the timeline of region and sex-specific age-related changes.

Our approach uses Grad-CAM analysis to highlight the spatial features that most strongly contributed to the age likelihood score for a given image. Here, we chose to present the heatmaps from two different layers of the model (the final convolutional layer of the 4th block of the second group of residual blocks and the final convolutional layer of the 3rd block of the final (fourth) group of residual blocks, respectively) to illustrate the spatial features important in the early and final stages of classification; however, the advantage of using Grad-CAM is that it can be applied to any convolutional layer in a neural network, which enables us to create a comparative set of maps that can provide a sense of the hierarchical feature extraction of the model from local to contextual, maximising the utility of our deep learning framework to provide the most comprehensive view of the features determining the model's decision making and enabling us to derive the most meaningful conclusions. The Grad-CAM images displayed here show that regions containing or adjacent to the blood vessel, including astrocyte endfeet, were important in the early stages of classification, while regions of the images containing the brain parenchyma were also important in the final stages of classification. Finally, as an additional functionality of this framework, we generated a score to better understand the findings of the model with respect to age for each sex and brain region. Our analysis shows that the model finds the greatest difference between young and aged BBB architecture in the prefrontal cortex (74.9%) and male mice (74.5%) (see Tables 2 and 3), respectively, which is in line with the literature published on both rodent and human brains.[17,29]

This study contains several strengths, as well as a few limitations that would also serve as focuses for future research. The use of deep learning techniques allows us to detect differences that might be difficult to observe on manual inspection, while ensuring greater objectivity in the findings. Automated analysis also greatly increases the number of images that can be analysed in a given time period. Furthermore, by harnessing the power of transfer learning, we were able to apply the knowledge obtained from training deep models on millions of natural images to our electron microscopy data, allowing us to achieve good performance with a comparatively small number of images (n=359). We compared four well-established architectures representing a balanced set of state-of-the-art (ResNet50), traditional (VGG16 and VGG19), and efficient (MobileNetv2) models for image classification, with all four models

equipped to handle diverse image types having been trained on the ImageNet database.[30–33] The final model used the ResNet50 architecture, a powerful deep network for learning complex, hierarchical features. This model provides a good first indication as to the differences in BBB architecture in young and aged mice; however, the required image input size of all four baseline models is 224-by-224 pixels. At this resolution, the model might struggle to capture fine-grained details unless they are large or distinct enough within the image. More domain-specific models (such as DenseNet121 and U-Net) might provide greater insight into age-related differences at a finer granularity.[34,35] However, these models are not typically designed for image classification and can introduce unnecessary complexity leading to overfitting. In addition, the use of such models is computationally expensive. As a key focus of this work has been to create a framework that can be used by experimentalists who may not have access to extensive computational resources, future directions would consider ensemble architectures that can leverage the generalisability and comparative computational efficiency of ResNet50 combined with the additional complexity of more specialised models.

In Supplementary Information Section 7, we discuss the model reliability and calibration and find that our model overestimates age likelihood, likely because of an imbalance in the data across brain regions. This motivates the applied age likelihood stratification which allows us to balance sensitivity and specificity with model uncertainty; however, in different research scenarios the trade-off between sensitivity and specificity should be re-evaluated to ensure the groups remain well calibrated for the task at hand. This work has focused on identifying age-associated changes in the architecture of the BBB in three different brain regions (see Supplementary Information Tables 3 in Supplementary Information Section 9 for a preliminary analysis of model performance across each brain region). Since our model is primarily designed for classification, it will first prioritise global patterns that are consistent across the whole dataset; however, by providing the model with anatomical information, we are providing the model with an explicit signal to treat different brain regions separately, so it may also learn to prioritise region-specific features that are important for the task of classification. Further work could look to apply our approach to datasets of electron microscopy images taken from single brain regions to improve our understanding of region-specific changes in BBB architecture.

Our feasibility study was conducted using electron microscopy images of brain tissue samples taken from wild-type murine models. Despite commonalities, there are a number of important age-related differences between mice and humans,[36] additional future work will investigate the utility of our model applied to human brains, as well inter-species differences in BBB architecture and the changes experienced during the ageing process.

Here, we provide preliminary evidence for an approach to identify the BBB architecture of aged brains which, with further testing, has the potential to accelerate research in the field of ageing and disease. The proposed model takes advantage of the advancements made in deep transfer learning to create a scalable and efficient framework that can be easily applied to a variety of datasets. Moreover, by applying stratification to our age likelihood scores, this allows us to modify group thresholds for different datasets and calibrate the model for improved performance in different research scenarios. Finally, Grad-CAM analysis (such as

in Figures 3 and 4) enables the presentation of explainable results, allowing researchers to understand which features most strongly contribute to the algorithm's final decision.

3BTRON is a deep transfer learning framework developed to enhance the analysis of BBB architecture in electron microscopy images. As an investigative tool, 3BTRON can be very powerful, offering researchers the possibility of more targeted manual analyses, focused on features highlighted by the model, such as the brain regions most susceptible to age-related changes, or the most relevant aspects of an image with respect to the class prediction for that image. The use of 3BTRON has the potential to help uncover key insights into the impact of ageing and neurodegenerative disease on the architecture of the BBB, accelerating research in biomarker and drug discovery for age-related diseases. Whilst this work focused on the BBB, this framework can be adapted to be applied to the investigation of other cell types and brain structures.

Methods

Study design and ethics

Electron microscopy images were obtained from C57Bl/6J mice. Animal experiments were conducted in accordance with the national and institutional guidelines ([Scientific Procedures Act] 1986 (UK), and the Council Directive 2010/63EU of the European Parliament and the Council of 22 September 2010 on the protection of animals used for scientific purposes) and had a full Home Office ethical approval. Mice were housed with no restrictions to food and water in a 12-hours light/dark cycle. The age of the mice was recorded at the time they were culled.

Electron Microscopy

Mice were perfused with PBS followed by fixative solution (4% paraformaldehyde w/v and 2% glutaraldehyde v/v in 0.1 M phosphate buffer). The brains were extracted, post-fixed in the same fixative solution for 24 hours at 4°C and sectioned into 50 μm thickness sections using a vibratome. Sections were post-fixed with 1% osmium tetroxide in 0.1 M phosphate buffer for 30 min, then dehydrated in ascending concentrations of ethanol dilutions (50%, 70 %, 95%, and 100%) and acetone. Sections were then immersed in resin and left to set overnight at room temperature. The sections were subsequently placed on microscope slides, covered with coverslips, and the resin was cured at 65°C for three days. The dissected areas were cut from the slides, mounted on plastic blocks, and ultrathin sectioned (60 nm thick) for electron microscopy. Each section was contrasted with lead citrate and uranyl acetate and imaged using a JOEL TEM-1400 plus electron microscope. Magnifications were selected to visualise each vessel along with the surrounding perivascular region for assessment.

Data characteristic and pre-processing procedures

In addition to image data, we also included sex and brain region data to the inference layer to allow for research interpretability and improve model performance and generalisability. In total, the dataset is comprised of 359 images, taken from 23 mice (11 female, 12 male). Of these images, 161 are from aged mice (mean age in days of 577, ± 40 to the nearest whole day) and 198 are from young mice (mean age in days of 98, ± 24 to the nearest whole day). Images were taken across three different brain regions: the corpus callosum (labelled CC), the hippocampus (labelled HC), and the prefrontal cortex (labelled PFC). Figure 1 shows a breakdown of the image data composition by demographics (age and sex) and anatomy (brain region), as well as a more detailed breakdown of sample distribution by mouse.

To make the input data compatible with our model, categorical data was transformed into a numeric format using one-hot encoding to avoid ordinal misinterpretation. To prepare the image data for our models, we performed a series of initial image-pre-processing steps to improve generalisability. We first used histogram equalisation to enhance contrast to make it easier for our models to distinguish key features. We then performed image thresholding to reduce noise, simplifying the image to further improve pattern recognition. Following this, standard pre-processing steps were used to ensure the image data matched the expectations of the pre-trained architectures tested during model development. The images were resized to 224 x 224 pixels, converted to an RGB format, and pixel values scaled to the range of [-1, 1], before being converted to a tensor.

Analysis Platform

All analyses were performed on a secure computing environment at Imperial College London using Python version 3.8.10. The Pandas[37] (version 2.2.1), NumPy[38] (version 1.26.4), Scikit-Learn[39] (version 1.4.2), and PyTorch[40] (version 2.2.2) packages formed much of our pipeline. All visualisations were plotted using Matplotlib[41] (version 3.8.4) and Seaborn[42] version (0.13.2).

Methodology

To ensure generalisability, the dataset was split into training and testing subsets in a 90:10 ratio, stratified by age. The training data represented 90% of the total data (n = 324 samples) and the testing data represented the remaining 10% (n = 35 samples). During model development and whilst optimising model hyperparameters and thresholds, validation sets were produced by splitting the training data using stratified k-fold cross-validation following the application of data shuffling. See Supplementary Information Figure 2 in Supplementary Information Section 4 for a visualisation of this evaluation. Stratification ensured that each fold contained a balanced representation of each age group compared to the whole training dataset, which is particularly important here due to the slight imbalance in the age group distributions, and data shuffling prevented ordering effects from influencing the model's performance. Following each split, the training set was augmented using a variety of

offline techniques (see Supplementary Information Section 2 for an in-depth discussion of the data augmentation techniques used), creating over a thousand examples of each class. We used sensitivity, specificity and the area under the precision-recall curve to measure model performance (for definitions of metrics, please see Supplementary Information Section 3).

Model development

We use transfer learning and combine image and categorical data to predict whether a vessel image comes from the brain tissue of a young or aged mouse based on the BBB architecture. Pre-trained models initialised with pre-trained weights are used for feature extraction. These image features are then concatenated with the categorical data to create a single unified vector which is then passed through a fully connected neural network to make the final prediction. For an in-depth illustration of the network architecture see Supplementary Information Figure 1 in Supplementary Information Section 1. We tested four commonly used deep learning models for image classification: ResNet50, MobileNetv2, VGG16, and VGG19.[30–33] These particular models all share the same input image data expectations with respect to image size, number of channels in the image, and pre-processing normalization) as they were all pre-trained on ImageNet. Hyperparameters were tuned using k-fold cross-validation (k = 10), with the model producing the highest precision-recall area under the curve score (on validation data) selected for the final analysis. See Supplementary Information Figure 2 in Supplementary Information Section 4 for a visualisation of this evaluation. Supplementary Information Section 5 contains information on the decisions made regarding each step of the model pipeline.

Stratification of probability estimates for reporting model uncertainty

Using an approach previously developed in our group,[43] probability estimates from the model are stratified into three groups (Green, Amber, and Red), which refer to low, medium, and high likelihood of the sample coming from an aged mouse, respectively. These groupings can be used as a measure of the model's uncertainty (how often the model is not confident in its predictions). By varying these thresholds, we can better balance levels of sensitivity and specificity with model uncertainty, allowing us to understand the key features that are used in the model's decision-making process for predicting the positive (aged) and negative (young) class, related to changes in the architecture of the BBB. This also allows our process to be flexible to different research scenarios and datasets.

Within this work, the optimal thresholds used in our final analysis were calculated using k-fold cross-validation (k = 5), using the model's predictions of the validation data after being re-trained with the best hyperparameters on the training data. See Supplementary Information Figure 2 in Supplementary Information Section 4 for a visualisation of this evaluation. We chose to use 5-fold cross-validation to prevent overfitting to the validation set by limiting the amount of model fine-tuning. This also reduced overhead, by balancing

validation with computational efficiency. More information on stratification is included in Supplementary Information Section 8.

Data Availability

The data presented in this study can be found on Zenodo at: https://doi.org/10.5281/zenodo.14845497.

Code Availability

To promote the sharing of resources, the final model, as well as all associated code, can be found on GitHub at https://github.com/tmi-lab/3BTRON. The code for experiments presented in this study will be made available by the corresponding author upon reasonable request.

References

[1] Sweeney MD, Zhao Z, Montagne A, Nelson AR, Zlokovic BV. Blood-Brain Barrier: From Physiology to Disease and Back. Physiological Reviews. 2019 Jan 1;99(1):21-78. Available from: https://www.ncbi.nlm.nih.gov/pubmed/30280653.

[2] Pan Y, Nicolazzo JA. Impact of aging, Alzheimer's disease and Parkinson's disease on the blood-brain barrier transport of therapeutics. Advanced Drug Delivery Reviews. 2018 Oct;135:62-74. Available from: https://dx.doi.org/10.1016/j.addr.2018.04.009.

[3] Banks WA, Reed MJ, Logsdon AF, Rhea EM, Erickson MA. Healthy aging and the blood–brain barrier. Nature Aging. 2021 Mar 1;1(3):243-54. Available from: https://www.ncbi.nlm.nih.gov/pubmed/34368785.

[4] Zhan R, Meng X, Tian D, Xu J, Cui H, Yang J, et al. NAD+ rescues aging-induced blood-brain barrier damage via the CX43-PARP1 axis. Neuron (Cambridge, Mass). 2023 Nov 15;111(22):3634-49.e7. Available from: https://search.proquest.com/docview/2863305519.

[5] Ádám Nyúl-Tóth, Tarantini S, DelFavero J, Yan F, Balasubramanian P, Yabluchanskiy A, et al. Demonstration of age-related blood-brain barrier disruption and cerebromicrovascular rarefaction in mice by longitudinal intravital two-photon microscopy and optical coherence tomography. American journal of physiology Heart and circulatory physiology. 2021 Apr 1;320(4):H1370-92. Available from: https://www.ncbi.nlm.nih.gov/pubmed/33543687.

[6] Yang AC, Stevens MY, Chen MB, Lee DP, Stähli D, Gate D, et al. Physiological blood–brain transport is impaired with age by a shift in transcytosis. Nature (London). 2020 Jul 16;583(7816):425-30. Available from: https://link.springer.com/article/10.1038/s41586-020-2453-z.

[7] Duncombe J, Lennen RJ, Jansen MA, Marshall I, Wardlaw JM, Horsburgh K. Ageing causes prominent neurovascular dysfunction associated with loss of astrocytic contacts and gliosis. Neuropathology and applied neurobiology. 2017 Oct;43(6):477-91. Available from: https://onlinelibrary.wiley.com/doi/abs/10.1111%2Fnan.12375.

[8] Ceafalan LC, Fertig TE, Gheorghe TC, Hinescu ME, Popescu BO, Pahnke J, et al. Age-related ultrastructural changes of the basement membrane in the mouse blood-brain barrier. Journal of cellular and molecular medicine. 2019 Feb;23(2):819-27. Available from: https://onlinelibrary.wiley.com/doi/abs/10.1111%2Fjcmm.13980.

[9] Hou Y, Dan X, Babbar M, Wei Y, Hasselbalch SG, Croteau DL, et al. Ageing as a risk factor for neurodegenerative disease. Nature reviews Neurology. 2019 Oct 1;15(10):565-81. Available from: https://link.springer.com/article/10.1038/s41582-019-0244-7.

[10] Agrawal S, Schneider JA. Vascular pathology and pathogenesis of cognitive impairment and dementia in older adults. Cerebral circulation - cognition and behavior. 2022 Jan 1;3:100148. Available from: https://dx.doi.org/10.1016/j.cccb.2022.100148.

[11] Farrall AJ, Wardlaw JM. Blood–brain barrier: Ageing and microvascular disease – systematic review and meta-analysis. Neurobiology of aging. 2009 Mar 1;30(3):337-52. Available from: https://www.clinicalkey.es/playcontent/1-s2.0-S0197458007002904.

[12] Montagne A, Barnes SR, Sweeney MD, Halliday MR, Sagare AP, Zhao Z, et al. Blood-Brain Barrier Breakdown in the Aging Human Hippocampus. Neuron. 2015 Jan 21;85(2):296-302. Available from: https://www.ncbi.nlm.nih.gov/pubmed/25611508.

[13] Juttukonda MR, Li B, Almaktoum R, Stephens KA, Yochim KM, Yacoub E, et al. Characterizing cerebral hemodynamics across the adult lifespan with arterial spin labeling MRI data from the Human Connectome Project-Aging. NeuroImage (Orlando, Fla). 2021 Apr 15;230:117807. Available from: https://dx.doi.org/10.1016/j.neuroimage.2021.117807.

[14] Bors L, Tóth K, Tóth EZ, Ágnes Bajza, Csorba A, Szigeti K, et al. Age-dependent changes at the blood-brain barrier. A Comparative structural and functional study in young adult and middle aged rats. Brain research bulletin. 2018 May;139:269-77. Available from: https://dx.doi.org/10.1016/j.brainresbull.2018.03.001.

[15] Bennett HC, Zhang Q, ting Wu Y, Manjila SB, Chon U, Shin D, et al. Aging drives cerebrovascular network remodeling and functional changes in the mouse brain. Nature communications. 2024 Jul 30;15(1):6398-20. Available from: https://link.springer.com/article/10.1038/s41467-024-50559-8.

[16] Alba C, Vidal L, Díaz F, Villena A, de Vargas IP. Ultrastructural and quantitative age-related changes in capillaries of the dorsal lateral geniculate nucleus. Brain Research Bulletin. 2004 Aug 30;64(2):145-53. Available from: https://dx.doi.org/10.1016/j.brainresbull.2004.06.006.

[17] Frías-Anaya E, Gromnicova R, Kraev I, Rogachevsky V, Male DK, Crea F, et al. Age-related ultrastructural neurovascular changes in the female mouse cortex and hippocampus. Neurobiology of aging. 2021 May;101:273-84. Available from: https://dx.doi.org/10.1016/j.neurobiolaging.2020.12.008.

[18] Garbuzova-Davis S, Haller E, Saporta S, Kolomey I, Nicosia SV, Sanberg PR. Ultrastructure of blood–brain barrier and blood–spinal cord barrier in SOD1 mice modeling ALS. Brain Research. 2007 Jul 9;1157:126-37. Available from: https://www.clinicalkey.es/playcontent/1-s2.0-S0006899307009729.

[19] LeCun Y, Bengio Y, Hinton G. Deep learning. Nature (London). 2015 May 28;521(7553):436-44. Available from: https://link.springer.com/article/10.1038/nature14539.

[20] Heckenbach I, Mkrtchyan GV, Ezra MB, Bakula D, Madsen JS, Nielsen MH, et al. Nuclear morphology is a deep learning biomarker of cellular senescence. Nature Aging. 2022 Aug 1;2(8):742-55. Available from: https://www.ncbi.nlm.nih.gov/pubmed/37118134.

[21] Alsenan S, Al-Turaiki I, Hafez A. A deep learning approach to predict blood-brain barrier permeability. PeerJ Computer science. 2021 Jun 10;7:e515. Available from: https://www.proquest.com/docview/2539743865.

[22] Aftab N, Masood F, Ahmad S, Rahim SS, Sanami S, Shaker B, et al. An optimized deep learning approach for blood-brain barrier permeability prediction with ODE integration. Informatics in medicine unlocked. 2024;48:101526. Available from: https://dx.doi.org/10.1016/j.imu.2024.101526.

[23] Huang ETC, Yang JS, Liao KYK, Tseng WCW, Lee CK, Gill M, et al. Predicting blood–brain barrier permeability of molecules with a large language model and machine learning. Scientific reports. 2024 Jul 9;14(1):15844-9. Available from: https://link.springer.com/article/10.1038/s41598-024-66897-y.

[24] Kumar R, Sharma A, Alexiou A, Bilgrami AL, Kamal MA, Ashraf GM. DeePred-BBB: A Blood Brain Barrier Permeability Prediction Model With Improved Accuracy.

Frontiers in neuroscience. 2022 May 3;16:858126. Available from: https://www.ncbi.nlm.nih.gov/pubmed/35592264.

[25] Mazumdar B, Sarma PKD, Mahanta HJ, Sastry GN. Machine learning based dynamic consensus model for predicting blood-brain barrier permeability. Computers in biology and medicine. 2023 Jun;160:106984. Available from: https://dx.doi.org/10.1016/j.compbiomed.2023.106984.

[26] Miao R, Xia LY, Chen HH, Huang HH, Liang Y. Improved Classification of Blood-Brain-Barrier Drugs Using Deep Learning. Scientific Reports. 2019 Jun 19;9(1):8802-11. Available from: https://link.springer.com/article/10.1038/s41598-019-44773-4.

[27] Selvaraju RR, Cogswell M, Das A, Vedantam R, Parikh D, Batra D. Grad-CAM: Visual Explanations from Deep Networks via Gradient-Based Localization. International Journal of Computer Vision. 2020 Feb 1;128(2):336-59. Available from: https://link.springer.com/article/10.1007/s11263-019-01228-7.

[28] Nation DA, Sweeney MD, Montagne A, Sagare AP, D'Orazio LM, Pachicano M, et al. Blood–brain barrier breakdown is an early biomarker of human cognitive dysfunction. Nature Medicine. 2019 Feb 1;25(2):270-6. Available from: https://link.springer.com/article/10.1038/s41591-018-0297-y.

[29] Shao X, Shou Q, Felix K, Ojogho B, Jiang X, Gold BT, et al. Age-related decline in blood-brain barrier function is more pronounced in males than females in parietal and temporal regions. eLife. 2024 Nov 4;13. Available from: https://www.ncbi.nlm.nih.gov/pubmed/39495221.

[30] He K, Zhang X, Ren S, Sun J. Deep Residual Learning for Image Recognition. IEEE; Dec 9, 2016. p. 770-8. Available from: https://ieeexplore.ieee.org/document/7780459.

[31] Sandler M, Howard A, Zhu M, Zhmoginov A, Chen LC. MobileNetV2: Inverted Residuals and Linear Bottlenecks. IEEE; Jun 2018. p. 4510-20. Available from: https://ieeexplore.ieee.org/document/8578572.

[32] Simonyan K, Zisserman A. Very deep convolutional networks for large-scale image recognition. arXiv (Cornell University). 2014 Sep 4. Available from: https://arxiv.org/abs/1409.1556.

[33] Deng J, Dong W, Socher R, Li LJ, Li K, Fei-Fei L. ImageNet: A large-scale hierarchical image database. IEEE; Jun 2009. p. 248-55. Available from: https://ieeexplore.ieee.org/document/5206848.

[34] Huang G, Liu Z, Maaten LVD, Weinberger KQ. Densely Connected Convolutional Networks. IEEE; Jul 2017. p. 2261-9. Available from: https://ieeexplore.ieee.org/document/8099726.

[35] Ronneberger O, Fischer P, Brox T. U-Net: Convolutional Networks for Biomedical Image Segmentation. Lecture Notes in Computer Science. 2015;9351:234-41. Available from: http://ebookcentral.proquest.com/lib/SITE_ID/reader.action?docID=5590589&ppg=259.

[36] Vanhooren V, Libert C. The mouse as a model organism in aging research: Usefulness, pitfalls and possibilities. Ageing Research Reviews. 2013 Jan 1;12(1):8-21. Available from: https://www.clinicalkey.es/playcontent/1-s2.0-S1568163712000542.

[37] McKinney W. Data Structures for Statistical Computing in Python. Proceedings of the Python in Science Conference. 2010;445:56-61. Available from: http://conference.scipy.org/proceedings/scipy2010/pdfs/mckinney.pdf.

[38] van der Walt S, Colbert SC, Varoquaux G. The NumPy Array: A Structure for Efficient Numerical Computation. Computing in Science & Engineering. 2011 Mar 1;13(2):22-30. Available from: https://ieeexplore.ieee.org/document/5725236.

[39] Pedregosa F, Varoquaux G, Gramfort A, Michel V, Thirion B, Grisel O, et al. Scikit-Learn: Machine Learning in Python. Journal of machine learning research. 2011 Oct 1. Available from: https://inria.hal.science/hal-00650905.

[40] Paszke A, Gross S, Massa F, Lerer A, Bradbury J, Chanan G, et al. PyTorch: An imperative style, high-performance deep learning library. arXiv (Cornell University). 2019 Dec 3. Available from: https://arxiv.org/abs/1912.01703.

[41] Hunter JD. Matplotlib: A 2D Graphics Environment. Computing in science & engineering. 2007 May 1;9(3):90-5. Available from: https://ieeexplore.ieee.org/document/4160265.

[42] Waskom M. Seaborn: statistical data visualization. Journal of open source software. 2021 Apr 6;6(60):3021. Available from: https://joss.theoj.org/papers/10.21105/joss.03021.pdf.

[43] Capstick A, Palermo F, Zakka K, Fletcher-Lloyd N, Walsh C, Cui T, et al. Digital remote monitoring for screening and early detection of urinary tract infections. NPJ digital medicine. 2024 Jan 13;7(1):11. Available from: https://link.springer.com/article/10.1038/s41746-023-00995-5.

Acknowledgements

This study is funded by the UK Dementia Research Institute [award number UK DRI-7002 and UK DRI-4007] through UK DRI Ltd, funded by the Medical Research Council (MRC), Alzheimer's Research UK, Alzheimer's Society, and the UKRI Engineering and Physical Sciences Research Council (EPSRC) PROTECT Project (grant number: EP/W031892/1), and

Alzheimer's Research UK (ARUK-NC2020-SCO). Katrine Gaasdal-Bech is a student on the Translational Neuroscience PhD Programme and is funded by Wellcome grant 218493/Z/19/Z. Infrastructure support for this research was provided by the NIHR Imperial Biomedical Research Centre (BRC), the UKRI Medical Research Council (MRC), and the funders were not involved in the study design, data collection, data analysis or writing the manuscript. Payam Barnaghi is also funded by the Great Ormond Street Hospital and the Royal Academy of Engineering.

Author Information

Authors and Affiliations

Here we list author affiliations.

Imperial College London, London, UK

Nan Fletcher-Lloyd & Payam Barnaghi

UK Dementia Research Institute, Care Research and Technology Centre, London, UK

Nan Fletcher-Lloyd & Payam Barnaghi

University College London, London, UK

Isabel Bravo-Ferrer • & Payam Barnaghi

Centre for Discovery Brain Sciences, The University of Edinburgh, Edinburgh, UK

Isabel Bravo-Ferrer •, Katrine Gaasdal-Bech & Blanca Díaz Castro

UK Dementia Research Institute, The University of Edinburgh, Edinburgh, UK

Isabel Bravo-Ferrer •, Katrine Gaasdal-Bech & Blanca Díaz Castro

British Heart Foundation and UK Dementia Research Institute Centre for Vascular Dementia Research, Edinburgh, UK

Katrine Gaasdal-Bech & Blanca Díaz Castro

Great Ormond Street Hospital NHS Foundation Trust, London, UK

Payam Barnaghi

• Isabel Bravo-Ferrer is currently affiliated with University College London but completed the work listed below at the Centre for Discovery Brain Sciences and UK Dementia Research Institute at the University of Edinburgh.

Contributions

NFL: Conceptualisation, Methodology, Software, Formal analysis, Investigation, Data Processing, Writing—Original Draft, Review and Editing, Visualisation; IBF, KGB: Data Collection, Review and Editing; BDC: Conceptualisation, Review and Editing, Supervision, Funding Acquisition; and PB: Conceptualisation, Methodology, Review and Editing, Supervision, Funding Acquisition.

Corresponding authors

Correspondence to Nan Fletcher-Lloyd

Ethics Declaration

Competing Interests

The authors declare no competing interests.